

# Absolute frequency and isotope shift of the magnesium $(3s^2) ^1S_0 \rightarrow (3s3d) ^1D_2$ two-photon transition by direct frequency-comb spectroscopy

E. Peters,<sup>\*</sup> S. Reinhardt,<sup>†</sup> Th. W. Hänsch,<sup>‡</sup> and Th. Udem<sup>§</sup>*Max Planck Institute of Quantum Optics (MPQ), Hans-Kopferman-Strasse 1, 85748 Garching, Germany*

(Received 11 August 2015; published 3 December 2015)

We use a picosecond frequency-doubled mode-locked titanium sapphire laser to generate a frequency comb at 431 nm in order to probe the  $(3s^2) ^1S_0 \rightarrow (3s3d) ^1D_2$  transition in atomic magnesium. Using a second, self-referenced femtosecond frequency comb, the absolute transition frequency and the  $^{24}\text{Mg}$  and  $^{26}\text{Mg}$  isotope shift is determined relative to a global-positioning-system-referenced hydrogen maser. Our result for the transition frequency of the main isotope  $^{24}\text{Mg}$  of 1 391 128 606.14(12) MHz agrees with previous measurements and reduces its uncertainty by four orders of magnitude. For the isotope shift we find  $\delta\nu^{26,24} = 3915.13(39)$  MHz. Accurate values for transition frequencies in Mg are relevant in astrophysics and to test atomic structure calculations.

DOI: [10.1103/PhysRevA.92.063403](https://doi.org/10.1103/PhysRevA.92.063403)

PACS number(s): 32.80.Rm, 78.47.N-, 42.65.Ky

## I. INTRODUCTION

The frequency comb [1] has been proven to be an excellent tool for precision spectroscopy. In the frequency domain the comb consists of a series of cw laser modes with frequencies  $\nu_n = n\nu_{\text{rep}} + \nu_0$  that are separated by the mode spacing  $\nu_{\text{rep}}$  but shifted from the exact harmonics of which by  $\nu_0$ . While detection and stabilization of  $\nu_{\text{rep}}$  is straightforward, detecting  $\nu_0$  requires beat notes between different harmonics of the comb (self-referencing). With that one can stabilize the two comb parameters to a radio frequency provided, for example, by an atomic clock. Beating a cw laser with a self-referenced comb yields its absolute frequency with the accuracy of the radio-frequency reference. Because self-referencing requires a large optical bandwidth, femtosecond lasers are usually employed.

A different usage of frequency combs is for spectroscopy, i.e., to directly probe an optical transition. This has several advantages if one wants to record a large spectral region at once, for example to investigate molecular spectra [2]. Unlike other broadband light sources a frequency comb may be resonantly coupled into a cavity for increased sensitivity [3]. On the other hand, it is also possible to use an individual mode to excite a spectrally isolated dipole-allowed transition in an atom [4]. While it is interesting to verify in this way that the individual modes of the comb indeed represent cw laser lines, this method is probably of limited practical use. One reason is the large number of nonresonant spectral modes, which possibly cause excess ac Stark shifts and background without contributing to the signal. The situation is quite different when exciting a two-photon transition with a frequency comb. In that case the energy of photons from pairs of modes may add up, such that the full power of all modes are used, while the linewidth of a single mode is maintained (see Fig. 1). The total excitation rate can be the same as that for a cw laser of the same average power [5]. However, there does not appear to be a real advantage over a cw laser unless no such laser exists [6–9]. The

large peak intensity of a pulse train that generates the frequency comb may be used to efficiently drive nonlinear processes to access short-wavelength regions. Depending on the type of nonlinearities and on the spectroscopic requirements, a picosecond mode-locked laser might be the better choice for this application, as detailed below.

A two-photon transition is well suited for precision spectroscopy. When two counterpropagating laser beams are used, their Doppler shifts add to zero in first order. The same applies to two-photon direct frequency comb spectroscopy with counterpropagating pulse trains. The line component that is free of the first-order Doppler shift is observed within the pulse collision volume. Just like with cw lasers, the time of flight of the atoms through the excitation volume gives rise to line broadening. While with cw lasers this effect occurs mainly for atomic trajectories that are transverse to the laser beams, with mode-locked lasers time-of-flight broadening also takes place for atomic trajectories longitudinal with the laser beams. With a sufficiently large pulse collision volume, a transition linewidth dominated by natural linewidth may be obtained with pulsed lasers [10,11].

The resonance condition for the Doppler-free component of a two-photon transition with an atomic frequency  $\nu_{eg}$  is given by

$$\nu_{eg} = 2\nu_0 + (n + m)\nu_{\text{rep}}, \quad (1)$$

with  $n$  and  $m$  being integer mode numbers of the comb. Mode pairs of the same  $\mu = n + m$  contribute to the same resonance that repeats with  $\nu_{\text{rep}}/2$  when referring to the laser frequency and with  $\nu_{\text{rep}}$  when measuring detuning at the atomic frequency  $\nu_{eg}$  as we do here. Therefore, the frequency comb can fix the transition frequency only modulo  $\nu_{\text{rep}}$  such that a coarse premeasurement or a combination of measurements with different repetition rates is used. The Doppler-free signal sits on a Doppler-broadened background created by the absorption of two photons from either direction. Due to its large width it can be assumed to be spectrally flat. Within the pulse collision volume the contrast between the Doppler-free signal and the Doppler-broadened background is given by the ratio of the corresponding linewidths multiplied by the number of modes within the Doppler width.

The excitation amplitudes of mode pairs with the same total energy expressed by Eq. (1) add coherently if the modes

<sup>\*</sup>Present address: GRS gGmbH.

<sup>†</sup>Present address: ENVINET GmbH, Haar, Germany.

<sup>‡</sup>Also at Ludwig-Maximilians-University, Munich, Germany.

<sup>§</sup>thu@mpq.mpg.de

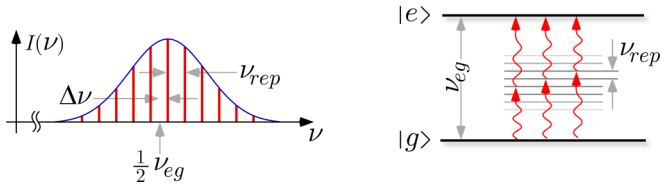


FIG. 1. (Color online) Direct frequency comb two-photon spectroscopy. Left: With one of the modes on resonance ( $\Delta\nu = 0$ ), all other modes may combine pairwise to deliver the atomic transition energy  $h\nu_{eg}$ . Right: For constructive interference of all excitation paths, the modes of the frequency comb must be properly phased. For nonresonant intermediate states this is the case with time bandwidth limited pulses at the center of the pulse collision volume. For atoms at rest a possible frequency chirp only decreases the excitation rate by approximately the time bandwidth product [12]. The corresponding longitudinal increase of the pulse collision volume may compensate that drop in signal [13].

are properly phased. This is exactly the case only at the center of the pulse collision volume for unchirped pulses. The usage of chirped pulses not only reduces the time-of-flight broadening for longitudinal atomic trajectories but also increases the number of contributing atoms in a gas. However, the corresponding dephasing reduces the excitation rates such that the better choice is to restrict the spectral bandwidth of the comb [12–15].

In astronomy, magnesium transitions act as an indicator for a possible drift of the fine structure constant with time [16] and for the metallicity of stars [17]. Neutral magnesium also offers the possibility to serve as a reference for an optical clock using the extremely sharp  $(3s^2)^1S_0 \rightarrow (3s3p)^1P_1$  intercombination line [18]. In atomic structure calculations magnesium—as the simplest and best studied two-valence-electron system—is often used as a testing ground for models using many-body methods [19,20]. New and improved spectroscopic data may greatly advance these models. Here we describe a measurement of the absolute frequency of the  $(3s^2)^1S_0 \rightarrow (3s3d)^1D_2$  two-photon transition at  $2 \times 431$  nm with a natural linewidth of 1.96(15) MHz [21]. This transition may provide additional information on the level structure, which is summarized in Fig. 2, and indirectly contributes to the above applications. It may also be used to improve calculations of binding energies and the first ionization energy from the Rydberg series [22]. A convenient way to generate 431 nm is by frequency-doubling either a semiconductor laser or a mode-locked titanium sapphire laser. In the latter case the doubling process is very efficient.

## II. EXPERIMENTAL SETUP

Our laser system is part of a setup that has been described previously [23]. We obtain 1.5 W of laser power at 862 nm from a ps mode-locked titanium sapphire laser (Spectra Physics, Tsunami) that is pumped with a 10-W cw laser at 532 nm (Coherent, Verdi V-10). Its pulse shape is best described by a  $\text{sech}^2$  profile with a measured duration of  $\approx 1.3$  ps and a spectral width of  $\approx 0.25$  THz indicating pulses close to the Fourier limit. A small fraction of the output power (200 mW) is used for stabilization, frequency measurement (fs frequency comb), and wavelength measurement ( $\lambda$  meter)

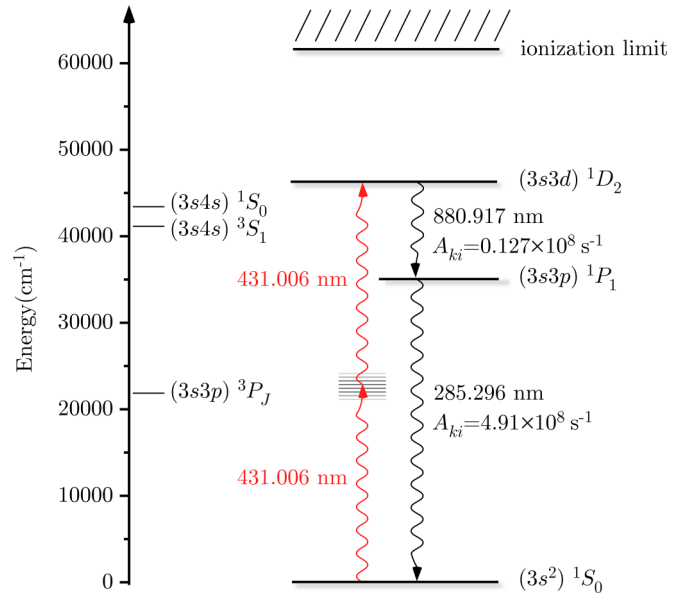


FIG. 2. (Color online) Magnesium levels relevant to this work. The  $(3s^2)^1S_0 \rightarrow (3s3d)^1D_2$  is excited by two 431-nm photons from a frequency comb and decays via the  $(3s3p)^1P_1$  level to the ground state by emitting an 881- and a 285-nm photon. The latter is used for detection. The natural linewidth of the  $(3s^2)^1S_0 \rightarrow (3s3d)^1D_2$  transition is 1.96 MHz [21]. The closely lying intermediate  $(3s3p)^3P_J$  triplet states ( $J = 0, 1, 2$ ) are weakly coupled to the laser (intercombination [18]) and in addition sufficiently far detuned ( $>38$  THz, ps comb not drawn to scale) to avoid stepwise single-photon excitation.

for determination of the mode number (see Fig. 3). The ps mode-locked laser is stabilized to an ultra-low-expansion (ULE) cavity with a free spectral range  $\nu_{\text{FSR}}$  of  $10\nu_{\text{rep}}$ , which is well isolated from acoustics and temperature variations. Using an electro-optic modulator (EOM), sidebands are imposed on each of the modes to generate the required error signal following the Pound-Drever-Hall method [24], which was used in transmission here [25]. At the same time the repetition rate is phase locked to a signal generator (Agilent, E8257D), which is referenced to a 10-MHz signal from a hydrogen maser that is continuously compared with a global positioning system (GPS) timing signal for calibration.

To tune the ps comb over the resonance a 200-MHz acousto-optic modulator (AOM) in double-pass configuration is placed in front of the ULE cavity. This allows its modes to shift by more than  $\nu_{\text{rep}}$ . The spectral envelope of the ps comb is measured using an optical spectrum analyzer (OSA; YOKOGAWA, AQ6319) and adjusted such that its peak coincides with the two-photon transition within an uncertainty of  $<0.02$  THz. A ps frequency comb does not have a sufficient bandwidth for self-referencing. For absolute frequency determination a cw semiconductor laser is phase locked with an offset of 20 MHz to one of the modes of the ps comb while beating against a mode of the self-referenced fs comb. This beat note is then recorded with a frequency counter (Agilent, 53131A). The repetition rate (800 MHz) and offset frequency (10 MHz) of the fs comb are controlled by the hydrogen maser.

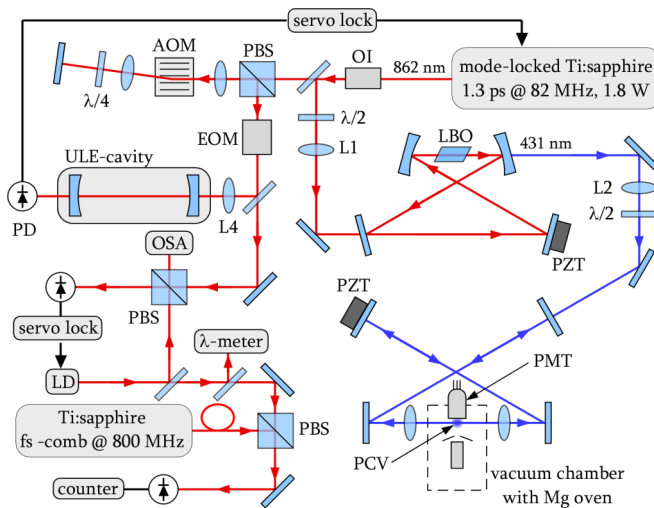


FIG. 3. (Color online) The setup for the Mg spectroscopy consists of a mode-locked ps titanium sapphire laser (“ps comb”) with a repetition rate of  $\sim 82$  MHz. This laser is resonantly enhanced for efficient frequency doubling and locked to an ULE cavity to narrow the linewidths of its modes. The frequency of one of its modes is measured by employing a second, self-referenced mode-locked fs titanium sapphire laser (“fs comb”) via a cw semiconductor laser (LD) that is used as a transfer oscillator. The mode number of the fs comb is determined with a  $\lambda$  meter. The spectroscopy takes place in a vacuum chamber that is filled with gas from a Mg oven. The vacuum chamber is surrounded by a second enhancement cavity that is resonant for the spectroscopy laser. Fluorescence is detected with a photomultiplier tube (PMT) via the 285-nm decay (see Fig. 2) that is extracted through a CaF window. OI, optical isolator; OSA, optical spectrum analyzer; PD, photodiode; AOM, acousto-optic modulator; EOM, electro-optic modulator; PBS, polarization beam splitter; PZT, piezoelectric transducer; PCV, pulse collision volume.

Frequency doubling of the ps comb is achieved by resonantly enhanced second-harmonic generation (SHG) using a Brewster-cut lithium triborate (LBO) crystal [26]. The ring resonator is stabilized with the help of the polarization method [27]. For the isotope shift measurement the free spectral range (FSR) of the cavity was set to twice the repetition rate of the ps comb. In this way, only every other mode is resonantly coupled into the SHG cavity, doubling the repetition rate at 431 nm while reducing the average output power accordingly. Thanks to the very good conversion efficiency for pulsed radiation, cavity losses are mainly conversion “losses” such that a moderate power enhancement of 4 still yields 230 mW averaged power at 431 nm. For absolute frequency measurements the FSR of the SHG cavity was matched to the pulse repetition rate of the ps comb. In this case every comb mode was resonantly coupled into the cavity and an average output power of 430 mW at 431 nm was obtained.

The spectrometer consists of another enhancement cavity that includes a vacuum chamber with a magnesium oven. To obtain a collision volume of the counterpropagating pulses, we employed a linear rather than a ring cavity, with twice the length of the SHG cavity. A half-wave plate in front of this cavity is used to control the orientation of the linear polarization. Two lenses with  $f = 750$  mm focal length inside the cavity generate a weak waist radius of  $w_0 =$

$132 \mu\text{m}$ . With an approximately perpendicular atomic beam, the time-of-flight broadening for a two-photon transition is given by  $\delta\nu = 2\bar{v}\sqrt{\ln(2)}/\pi w_0 = 3.41$  MHz using the rms thermal velocity of  $\bar{v} = 850$  m/s at  $T = 700$  K. Modulating the cavity length at 96 kHz with a piezoelectric transducer (PZT) mounted mirror and demodulating the transmitted light with a lock-in amplifier allows one to generate an error signal to lock the cavity to the laser by feeding back on the same PZT. The total round-trip losses of this resonator were measured to be 28.4% and in combination with an input coupler of 88% reflectivity an enhancement of 2 is achieved. For spectroscopy, more important than the enhancement is the spatial mode matching of the counterpropagating pulse trains. Even a low-finesse cavity is quite efficient for this purpose because it enhances the mode-matched part while attenuating (reflecting) the nonmatched fraction.

Two antireflection coated windows allowed the laser beam to pass through the vacuum chamber. A third CaF<sub>2</sub> window on top of the vacuum chamber was used for detection of the fluorescence at 285 nm. An imaging system was placed behind the detection window which mapped the pulse collision volume through a 3-mm aperture onto the cathode of a photomultiplier tube (PMT; Hamamatsu, R6358). Background light was suppressed using a combination of a colored glass filter (Shott, UG11) and an interference filter (Asahi Spectra, MC28J3) with 14% total transmission at 285 nm. Taking the quantum efficiency of the PMT (23%) and the detected solid angle (0.04 of  $4\pi$ ) into account, the total detection efficiency is estimated to be around  $1 \times 10^{-4}$ . To compensate for stray magnetic fields within the pulse collision volume, three pairs of coils were placed around the vacuum chamber. While the magnetic field inside the vacuum chamber was monitored using a Forster probe, it was reduced to less than  $20 \mu\text{T}$ , with the magnesium oven switched off. The magnetic field generated by the magnesium oven at the interaction volume in 10 mm distance is estimated to  $10 \mu\text{T}$  (see below).

The magnesium oven consists of a 10-mm-long tube with a diameter of 1 mm filled with a piece of magnesium wire. While the back end of the tube is sealed, the front end is placed at a distance of 10 mm from the center of the pulse collision volume. A three-loop tantalum wire is wrapped around the tube. By applying an electrical current of 5–6 A to this wire, the oven is heated to around 700 K, which corresponds to a vapor pressure of  $1 \times 10^{-4}$  to  $1 \times 10^{-2}$  mbar [28]. During the measurement the pressure inside the vacuum chamber was kept below  $1 \times 10^{-5}$  mbar. A skimmer in front of the magnesium oven reduced the beam spread, and additional apertures inside the vacuum chamber protected the laser and detection windows from being coated with magnesium. The operation of the magnesium oven was not continuous at all times, presumably due to oxide layers on the wire resulting in bursts and drops of the observed Mg density. We used magnesium with a natural abundance of three stable isotopes:  $^{24}\text{Mg}$ : $^{25}\text{Mg}$ : $^{26}\text{Mg}$ =79%:10%:11%. The even nuclei  $^{24}\text{Mg}$  and  $^{26}\text{Mg}$  have no nuclear spin and thus show no hyperfine structure (HFS).  $^{25}\text{Mg}$ , however, has a nuclear spin of  $I = 5/2$  and the excited state  $^1D_2$  splits into five hyperfine levels which leads to at least three-times-weaker line strengths per component. These components are not unambiguously seen in our data (see Fig. 4). Given the atomic and laser parameters we estimate

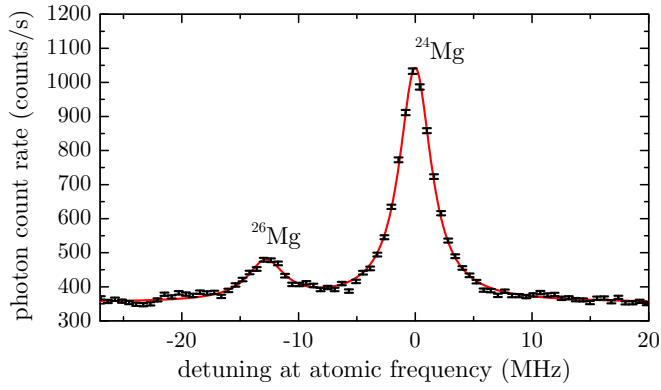


FIG. 4. (Color online) Magnesium  $(3s^2)^1S_0 \rightarrow (3s3d)^1D_2$  excited with a ps frequency comb and detected via the  $(3s3d)^1D_2 \rightarrow (3s3p)^1P_1 \rightarrow (3s^2)^1S_0$  decay at 285 nm. The frequency comb is tuned by scanning a double-pass acousto-optic modulator (AOM) that is placed between the ps mode-locked laser and its reference cavity (see Fig. 3). The AOM frequency enters the optical atomic frequency with a factor of 8 as the ps comb is tuned by a double-pass AOM, is frequency doubled, and then excites a two-photon transition. The smaller peak at the left is identified with the  $^{26}\text{Mg}$  isotope (abundance 11%) while the right peak belongs to  $^{24}\text{Mg}$  (abundance 79%). The  $^{25}\text{Mg}$  (abundance 10%) line is split into five weaker hyperfine components that are not detected in this experiment. The solid red line is the fit result of a sum of two real-valued Lorentzian functions with a constant offset. From this fit we find a full width at half maximum of 3.47(6) MHz for  $^{24}\text{Mg}$  in reasonable agreement with the natural linewidth combined with the estimated time-of-flight broadening. Because the frequency comb is folded into the line structure, an integer multiple of  $\nu_{\text{rep}} = 81.8338$  MHz needs to be added to the line splitting to obtain the isotope shift.

the Doppler-free to Doppler-broadened contrast to 28. Since a considerable part of the fluorescence is collected from outside the pulse collision volume and the unseen hyperfine components add, the background is much larger.

### III. RESULTS

To determine the  $^{26}\text{Mg}$  and  $^{24}\text{Mg}$  isotope shift of the  $(3s^2)^1S_0 \rightarrow (3s3d)^1D_2$  transition from the recorded fluorescence shown in Fig. 4 we fit a sum of two real-valued Lorentzian functions to the data with a constant offset that takes care of the Doppler-broadened background. Since the periodic structure of the ps comb is folded into this line shape, an integer multiple of the pulse repetition rate, that is not known *a priori*, needs to be added to the result:

$$\delta\nu^{26,24} = 8(\nu_{24\text{Mg}}^{\text{AOM}} - \nu_{26\text{Mg}}^{\text{AOM}}) + \mu\nu_{\text{rep}}. \quad (2)$$

Here the experimental line positions are expressed through relative AOM frequencies at which they occur.

The integer  $\mu$  is an even number, because the SHG cavity acts as a filter cavity and doubles  $\nu_{\text{rep}}$ . It is determined by carrying out the measurement with slightly different repetition rates, requiring that the same value for the isotope shift is obtained. Not all values of  $\nu_{\text{rep}}$  are equally suited. A restriction enters because of the stabilization scheme of the ps comb. To obtain a useful error signal from the ULE cavity, its free spectral range ( $\nu_{\text{FSR}}$ ) and  $\nu_{\text{rep}}$  need to be at a not-too-large

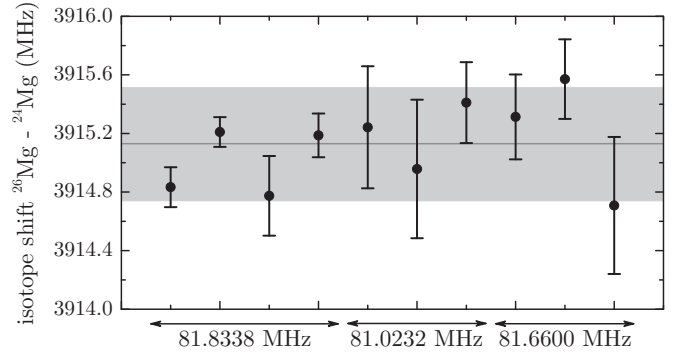


FIG. 5. Magnesium  $(3s^2)^1S_0 \rightarrow (3s3d)^1D_2$  isotope shift between  $^{26}\text{Mg}$  and  $^{24}\text{Mg}$  measured with different repetition rates of the ps comb ( $\nu_{\text{rep}} = 81.8338$ ,  $81.0232$ , and  $82.6600$  MHz). Each value is obtained from around ten line scans such as the one in Fig. 4. The statistical error bars are determined from the fit. The weighted mean (horizontal line) of this data set is  $\delta\nu^{26,24} = 3915.13(39)$  MHz with the total uncertainty given by the shaded region.

integer ratio. We used repetition rates of 81.8338 MHz ( $\approx \nu_{\text{FSR}}/10$ ), 81.0232 MHz ( $\approx \nu_{\text{FSR}}/10.1$ ), and 82.6600 MHz ( $\approx \nu_{\text{FSR}}/9.9$ ). Only  $\mu = 48$  in all three cases leads to an agreement of the isotope shift within 1 MHz according to Eq. (2).

The overall results for the isotope shift measurement are summarized in Fig. 5 with statistical error bars determined from the weighted fits. Every data point represents a run with several successive scans. Scans where the laser was out of mode lock or the spectroscopy cavity was out of lock as well as scans with an almost empty Mg oven have been discarded. This left us with typically ten suitable scans for each of the ten runs that are presented in Fig. 5. The Birge ratio (square root of the reduced  $\chi^2$ ) of this data is 1.2 and indicates small fluctuating systematic effects which may be explained by line distortions from undetected  $^{25}\text{Mg}$  HFS components. To get an upper limit on this effect we fit two real-valued Lorentzian functions to simulated  $^{24}\text{Mg}$  and  $^{26}\text{Mg}$  lines and record the line spacing while sweeping  $^{25}\text{Mg}$  lines over the resonances. In this way we find a maximum systematic uncertainty of the isotope shift between  $^{26}\text{Mg}$  and  $^{24}\text{Mg}$  of 380 kHz. Other systematic effects such as the ac Stark and Zeeman effects are common to both lines, leaving the isotope shift unaffected. We compute the weighted mean over the ten runs and determine the statistical uncertainty of that mean to 70 kHz. Our final result for the isotope shift between  $^{26}\text{Mg}$  and  $^{24}\text{Mg}$  and its total uncertainty (shaded area in Fig. 5) is

$$\delta\nu^{26,24} = 3915.13(39)\text{MHz}. \quad (3)$$

Our value lies about 1.5 combined standard deviations below the theoretical value of 3.96 GHz which has an uncertainty of approximately 20–30 MHz due to the neglected volume-effect term [20].

Ignoring the volume-effect term we can approximately compute the unmeasured isotope shift between  $^{25}\text{Mg}$  and  $^{24}\text{Mg}$  from the measured isotope shift between  $^{26}\text{Mg}$  and  $^{24}\text{Mg}$ :

$$\begin{aligned} \delta\nu^{25,24} &= \frac{m_{26}(m_{25} - m_{24})}{m_{25}(m_{26} - m_{24})} \delta\nu^{26,24} \\ &= 0.520988 \delta\nu^{26,24} = 2040 \text{ MHz}. \end{aligned} \quad (4)$$

In this expression the theoretical coefficients for the normal and the specific mass shift cancel and the scaling factor for the isotope shift is determined by the masses of the three isotopes,  $m_{24}$ ,  $m_{25}$ , and  $m_{26}$  [29]. The uncertainty of this isotope shift is dominated by the uncalculated volume-effect term which, upon multiplying with the mass ratio above, reduces to 10–15 MHz. In contrast to the even isotopes the excited state of  $^{25}\text{Mg}$  is subject to hyperfine splitting. Because  $J = 0$  there is only one hyperfine level ( $F = 5/2$ ) in the ground state while there are five of them in the excited state. Their intensities increase linearly with  $F$  and reach one-third of the even isotope intensity (if all isotopes had equal abundances) [30]. The hyperfine constants were measured in Ref. [31] but the sign given there does not seem to be consistent with the presented spectrum (Fig. 7 in Ref. [31]). Therefore, we do not use these constants here to compute the frequencies of the individual hyperfine components of  $^{25}\text{Mg}$ .

The absolute atomic frequency can be expressed in terms of the experimentally accessible frequencies:

$$\nu_{eg} = 1\,391\,248\,346\,000 \text{ kHz} + 8\nu_{^{24}\text{Mg}}^{\text{AOM}} + \mu\nu_{\text{rep}}, \quad (5)$$

where the large optical offset frequency is set by the GPS-referenced hydrogen maser that controls the frequency of the cw semiconductor laser via the fs comb (see Fig. 3). Its uncertainty is below 100 Hz and therefore negligible for this experiment. Just like in Eq. (2) an integer multiple (not necessarily even) of the repetition rate needs to be added to the measured value which is determined as described above. The final precision measurements were carried out with a fixed repetition frequency of  $\nu_{\text{rep}} = 81.8338$  MHz.

The absolute frequency of the ps comb is determined in two steps. First the drift of the ULE reference resonator is determined with the help of the fs comb. A linear fit to this frequency as a function of time then allows one to average out the short-term instability of the hydrogen maser. The linear function is used to determine the absolute frequency that corresponds to each time-tagged fluorescence data point. The overall result of the absolute frequency measurement is summarized in Fig. 6. Every data point represents a run with up to 43 successive scans with the same criteria for discarding unsuitable data as above. The Birge ratio of the data is 2.6,

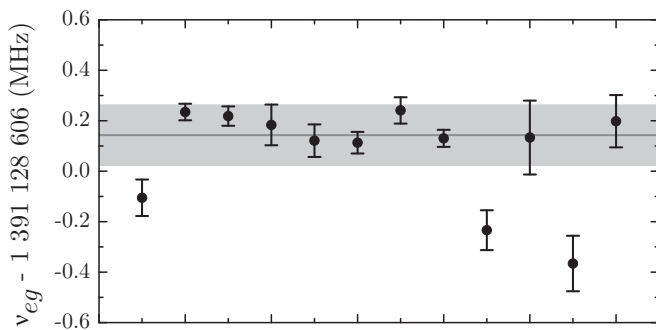


FIG. 6.  $^{24}\text{Mg} (3s^2) ^1S_0 \rightarrow (3s3d) ^1D_2$  transition frequency. Each of the values is obtained from several line scans such as the one in Fig. 4 with a statistical error bar determined from the fits. These error bars indicate additional systematic effects that are taken into account to determine the overall uncertainty (shaded area) of the weighted mean  $\nu_{eg} = 1\,391\,128\,606.14(12)$  MHz (horizontal line).

indicating significant fluctuating systematic effects that we attribute to instabilities of the magnesium vapor pressure as described above. To take this effect into account we multiply the statistical uncertainty of the mean by the Birge ratio and obtain 90 kHz.

The absolute frequency is sensitive to additional systematic effects. The line distortion due to the undetected  $^{25}\text{Mg}$  HFS lines is estimated in the above manner to cause a shift of up to 46 kHz. This type of uncertainty is now much smaller because the strong  $^{24}\text{Mg}$  resonance is less sensitive. With a total angular momentum of  $J = 2$  the excited state splits symmetrically into five Zeeman levels with a maximum shift of 28 MHz/mT. Adding the residual stray fields and the field generated by the oven yields  $30 \mu\text{T}$ . With a measured maximum imbalance of the polarization of up to 14% we estimate the Zeeman shift by the same fraction to be 59 kHz. The ac Stark shift for the given experimental conditions (average power  $P = 860$  mW per direction, radial average intensity  $P/\pi w_0^2$ ) is calculated to be 14 kHz, using the dipole matrix elements in Ref. [32] which yield an approximate shift of  $2.2 \times 10^{-4}$  Hz  $\text{m}^2/\text{W}$ . We treat this effect as an uncertainty. With the magnesium oven at a temperature of around 700 K we compute a rms velocity of 850 m/s assuming a Maxwellian velocity distribution. From this the second-order Doppler shift is estimated to 6 kHz, which is also treated as an uncertainty. The small modulation of the spectroscopy cavity with 96 kHz and a 0.35-nm (0.350-V) amplitude caused a shift of the transition frequency by 0.6 kHz. Even though the usage of chirped laser pulses does not cause a systematic shift for atoms at rest, it can give rise to such a shift for a diverging atomic beam. We estimate this effect by computing the spectrum of the two-photon Rabi frequency in the atomic rest frame in combination with geometric restrictions of the atomic beam and the detector field of view (radius  $\approx 1.5$  mm). Using an upper limit of the chirp parameter of 0.5 from the quality of the measured time bandwidth product, we find a maximum systematic shift of 22 kHz due to this effect. Combining all uncertainties we obtain for the  $^{24}\text{Mg} (3s^2) ^1S_0 \rightarrow (3s3d) ^1D_2$  transition frequency

$$\nu_{eg} = 1\,391\,128\,606.14(12) \text{ MHz}, \quad (6)$$

which is in excellent agreement with an earlier measurement but four orders of magnitude more accurate [33,34].

#### IV. CONCLUSION

In summary the isotopic shift between  $^{26}\text{Mg}$  and  $^{24}\text{Mg}$  and the absolute frequency of the  $(3s^2) ^1S_0 \rightarrow (3s3d) ^1D_2$  two-photon transition were measured with an uncertainty that is comparable to and better than other measurements from the ground state in Mg [18,35,36]. These results can help to improve the understanding of the Mg spectrum and also the spectroscopy with frequency combs generated by nonlinear processes in crystals.

#### ACKNOWLEDGMENTS

This research was supported by the German Research Foundation (DFG) cluster of excellence ‘‘Munich Centre for Advanced Photonics (MAP).’’ Th.W.H. acknowledges support by the Max Planck Foundation.

- [1] T. Udem, R. Holzwarth, and T. W. Hänsch, *Nature (London)* **416**, 233 (2002).
- [2] M. C. Stowe, M. J. Thorpe, A. Pe'er, J. Ye, J. E. Stalnaker, V. Gerinov, and S. A. Diddams, *Adv. At. Mol. Opt. Phys.* **55**, 1 (2008).
- [3] B. Bernhardt, A. Ozawa, P. Jacquet, M. Jacquy, Y. Kobayashi, Th. Udem, R. Holzwarth, G. Guelachvili, T. W. Hänsch, and N. Picque, *Nat. Photonics* **4**, 55 (2010).
- [4] V. Gerginov, C. E. Tanner, S. A. Diddams, A. Bartels, and L. Hollberg, *Opt. Lett.* **30**, 1734 (2005).
- [5] Ye. V. Baklanov and V. P. Chebotayev, *Appl. Phys.* **12**, 97 (1977).
- [6] M. Herrmann, M. Haas, U. D. Jentschura, F. Kottmann, D. Leibfried, G. Saathoff, C. Gohle, A. Ozawa, V. Batteiger, S. Knünz *et al.*, *Phys. Rev. A* **79**, 052505 (2009).
- [7] S. Witte, R. Th. Zinkstok, W. Ubachs, W. Hogervorst, and K. S. E. Eikema, *Science* **307**, 400 (2005).
- [8] A. Cingöz, D. C. Yost, T. K. Allison, A. Rühl, M. E. Fermann, I. Hartl, and J. Ye, *Nature (London)* **482**, 68 (2012).
- [9] A. Ozawa and Y. Kobayashi, *Phys. Rev. A* **87**, 022507 (2013).
- [10] M. J. Snadden, A. S. Bell, E. Riis, and A. I. Ferguson, *Opt. Commun.* **125**, 70 (1996).
- [11] P. Fendel, S. D. Bergeson, Th. Udem, and T. W. Hänsch, *Opt. Lett.* **32**, 701 (2007).
- [12] S. Reinhardt, E. Peters, T. W. Hänsch, and Th. Udem, *Phys. Rev. A* **81**, 033427 (2010).
- [13] A. Ozawa and Y. Kobayashi, *Phys. Rev. A* **86**, 022514 (2012).
- [14] B. Broers, H. B. van Linden van den Heuvell, and L. D. Noordam, *Opt. Commun.* **91**, 57 (1992).
- [15] D. Meshulach and Y. Silberberg, *Nature (London)* **396**, 239 (1998).
- [16] V. V. Flambaum, *Eur. Phys. J. Spec. Top.* **163**, 159 (2008).
- [17] M. J. Ruck and G. Smith, *Astron. Astrophys.* **277**, 165 (1993).
- [18] J. Friebe, A. Pape, M. Riedmann, K. Moldenhauer, T. Mehlstäubler, N. Rehbein, C. Lisdat, E. M. Rasel, W. Ertmer, H. Schnatz *et al.*, *Phys. Rev. A* **78**, 033830 (2008).
- [19] J. C. Berengut, V. A. Dzuba, V. V. Flambaum, and M. G. Kozlov, *Phys. Rev. A* **69**, 044102 (2004).
- [20] J. C. Berengut, V. V. Flambaum, and M. G. Kozlov, *Phys. Rev. A* **72**, 044501 (2005).
- [21] G. Jönsson, S. Kröll, A. Persson, and S. Svanberg, *Phys. Rev. A* **30**, 2429 (1984).
- [22] M. Rafiq, M. A. Kalyar, and M. A. Baig, *J. Phys. B* **40**, 3181 (2007).
- [23] E. Peters, S. A. Diddams, P. Fendel, S. Reinhardt, T. W. Hänsch, and Th. Udem, *Opt. Express* **17**, 9183 (2009).
- [24] R. W. P. Drever, J. L. Hall, F. V. Kowalski, J. Hough, G. M. Ford, A. J. Munley, and H. Ward, *Appl. Phys. B* **31**, 97 (1983).
- [25] M. Houssin, M. Jardino, and M. Desaintfuscien, *Rev. Sci. Instrum.* **61**, 3348 (1990).
- [26] M. Watanabe, R. Ohmukai, K. Hayasaka, H. Imajo, and S. Urabe, *Opt. Lett.* **19**, 637 (1994).
- [27] T. W. Hänsch and B. Couillaud, *Opt. Commun.* **35**, 441 (1980).
- [28] C. B. Alcock, V. P. Itkin, and M. K. Horrigan, *Can. Metall. Q.* **23**, 309 (1984).
- [29] G. Audi, M. Wang, A. H. Wapstra, F. G. Kondev, M. Maccormick, X. Xu, and B. Pfeiffer, *Chin. Phys. C* **36**, 1603 (2012).
- [30] G. Grynberg, F. Biraben, E. Giacobino, and B. Cagnac, *J. Phys.* **38**, 629 (1977).
- [31] R. Beigang and A. Timmermann, *J. Phys.* **44**, 137 (1983).
- [32] S. G. Porsev, M. G. Kozlov, Yu. G. Rakhlina, and A. Derevianko, *Phys. Rev. A* **64**, 012508 (2001).
- [33] G. Risberg, *Ark. Fys.* **28**, 381 (1965).
- [34] D. C. Martin and R. Zalubas, *J. Phys. Chem. Ref. Data* **9**, 1 (1980).
- [35] E. J. Salumbides, S. Hannemann, K. S. E. Eikema, and W. Ubachs, *Mon. Not. R. Astron. Soc.* **373**, L41 (2006).
- [36] S. Hannemann, E. J. Salumbides, S. Witte, R. Th. Zinkstok, E. J. van Duijn, K. S. E. Eikema, and W. Ubachs, *Phys. Rev. A* **74**, 012505 (2006).